Real-Time Liver Tumor Detection with a Multi-Class Ensemble Deep Learning Framework

Nanda Prakash Nelaturi
Department of ECE, Koneru Lakshmaiah Education Foundation, India
nandaprakashnelaturi@gmail.com (corresponding author)

Vullanki Rajesh
Department of ECE, Koneru Lakshmaiah Education Foundation, India
rajesh4444@kluniversity.in

Inthiyaz Syed
Department of ECE, Koneru Lakshmaiah Education Foundation, India
syedinthiyaz@kluniversity.in

Received: 12 June 2024 | Revised: 21 June 2024 and 28 June 2024 | Accepted: 3 July 2024

 DOI: https://doi.org/10.48084/etasr.8106

ABSTRACT

Detecting liver tumors in large heterogeneous datasets is vital for accurate diagnosis and treatment to be performed. However, existing segmentation models struggle with multimodal tumor detection, variability in tumor shapes, over-segmentation, and noise in border regions. These issues lead to inconsistent and inaccurate results. The current study introduces a novel multiclass ensemble feature extraction and ranking-based deep learning framework to address these challenges. This framework efficiently identifies key tumor regions with a high true positive rate and maintains runtime efficiency, making it suitable for real-time liver tumor detection. Comparative evaluations using diverse liver imaging databases demonstrate the framework's superiority over existing models in terms of various classification metrics and runtime efficiency. These results highlight the framework's potential for enhancing real-time liver tumor detection applications.

Keywords-multi-variate liver filtering; multi-class liver segmentation; ensemble deep learning classifiers

I. INTRODUCTION

Liver and tumor image segmentation is an exciting research area that relies on collaboration between engineers and physicians. Utilizing medical imaging techniques offers invaluable insights for diagnosing and planning treatments for liver diseases, including tumor detection [1]. Collaborations extend across research institutes to effectively address biomedical research problems. Diverse hardware and software solutions have been developed to analyze biomedical data, with medical imaging playing a pivotal role in various fields of research and therapy. Researchers analyze images of different modalities, employing contemporary visualization methods [2]. Traditional approaches to identifying abnormal growths within the liver, such as tumors, require significant human involvement, leading to time constraints, especially for large populations. Thus, an automated method becomes imperative for timely liver tumor detection. Analyzing the functional insufficiency of liver cancer patients involves identifying the location and type of cancer lesions. The accurate classification of liver cancer types by clinicians for appropriate treatment heavily depends on early and precise lesion examination [3]. The primary objective of diagnostic methods is to detect cancer presence and accurately delineate cancerous tissue types.

Currently, physicians use various imaging modalities to diagnose and treat liver cancer. Computed Tomography (CT) scans are an affordable and widely employed technique for identifying cancerous regions. CT scans offer excellent spatial resolution and can comprehensively examine the entire liver in a single slice, which makes them optimal for abdominal diagnostics. Advanced CT technologies, such as helical CT and multi-detector row helical CT, have emerged, providing superior picture resolution and faster image acquisition compared to typical CT scanners, thereby enhancing diagnostic capabilities in liver tumor imaging research. In liver anatomy research, diverse CT images provide researchers with valuable insights, facilitating precise analysis. Medical imaging is an integral part of diagnostic methods, where clinicians employ computer-aided processes to guide the monitoring of disease progression [4-6]. The analysis of medical images is essential for accurate identification and prediction of malignant cells. Biomedical image segmentation, a complex domain within image processing, plays a crucial role. Segmentation divides images into uniform sections based on intensity attributes,

aiding in the detection of tumors and pathological abnormalities in organs.

Image segmentation helps physicians accurately identify lesions, which is crucial for early cancer detection in oncology. Conventional manual segmentation techniques often fail to identify the smallest areas within CT scans. Therefore, the use of automated segmentation algorithms is imperative for precise cancer lesion detection during CT scan data processing [7]. Previous studies have focused extensively on CLIVER systems for identifying cancerous lesions in liver CT scans. Various segmentation approaches, including edge-based, region-based [8], thresholding [9], and clustering-based [10] methods, have been presented. Figure 1 shows different shapes and orientations of liver tumors in large databases.

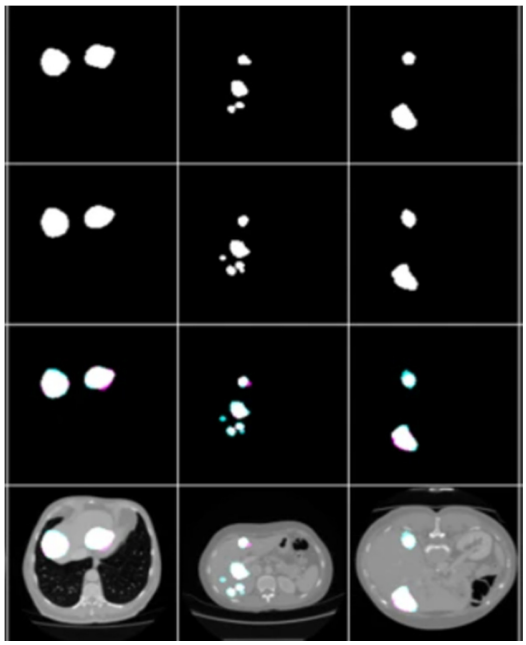

Fig. 1. Different shapes and orientations of liver tumors in large databases.

In the realm of liver and tumor image segmentation, methods leveraging edge or contour detection often utilize statistical and geometrical active shape models. A liver segmentation technique, combining the level set method with the watershed transform, achieved a segmentation accuracy of 92% [11]. The vibrating level setting method has displayed that employing a maximum number of filters produces superior segmentation results [12]. An automated Computer-Aided Design (CAD) method focused on diagnosing liver disorders, including cysts, hemangiomas, hepatocellular carcinoma, and focal metastatic liver disorders using ultrasound images [13]. Liver disorders and malignancies can be distinguished in ultrasound pictures [14]. Region-based segmentation algorithms group pixels based on similar properties, employing either region-growth or region-splitting approaches. Volumetric region growth deploys automated 3D seed point selection with threshold values for automatic stop conditions [15]. In [16], a confidence-connected region growth approach was proposed to autonomously segment liver and cancer lesions on CT images, evaluating results against manual segmentation using various measurement factors. In [17], three semi-automatic seeded region-growth methods were presented for liver tumor segmentation: 2D region-growing with constraints, proportional learning with 2D voxel classification, and Bayesian rule with 3D region-growing. In [18-19], different methods for breast cancer detection were introduced.

This study proposes a dynamic multivariate multi-region tumor filtering approach for feature extraction and tumor segmentation on a real-time database.

II. MULTI-VARIATE LIVER AND TUMOR SEGMENTATION AND CLASSIFICATION

A. Multivariate Liver Data Filtering

In liver image analysis, liver image filtering is substantial for feature selection, denoising, and compression. Sparse filtering works well in eliminating sparse noise, but frequently misses intricate relationships and data structures. This is addressed by Multi-variate Non-linear Gaussian Estimation (MNGE), which makes it possible to describe non-linear relationships by estimating the parameters of a non-linear Gaussian model. MNGE can be combined with sparse filtering to produce a non-linear Gaussian model with sparsity.

To appropriately describe the distribution of liver image data, the method begins with the estimation of non-linear Gaussian parameters using MNGE. After sparse noise has been eliminated, sparse filtering is applied to keep important features and eliminate unnecessary ones, improving the accuracy of further analysis. Depending on the features of the dataset and the intended results, several techniques are followed to implement MNGE and sparse filtering. For MNGE, these techniques include variational Bayesian or expectation-maximization algorithms, while for sparse filtering, they entail L1 regularization or sparse coding. This combination method improves the detection of liver diseases and hepatic image analysis for better diagnostic results. Liver image filtering increases the accuracy of analysis by removing features and noise from liver image datasets. The steps involved in the filtering process are listed below.

1) Initialize Variables

Input: Liver image dataset $\mathcal{D}$, initial parameters θ_0.

Initialize: Normalized Laplacian Graph (NLG) calculations, observed and expected frequency calculations.

2) Calculate Normalized Laplacian Graph (NLG)

For each numerical feature f in $\mathcal{D}$:NLG = $\max\{\lambda \mid \lambda \leq \epsilon\}$, where ϵ is a user-defined parameter.

3) Probabilistic GMM

For non-fatty liver samples, the probability that a tumor's characteristics (s_i) belong to the GMM is represented by the GMM as $\_nf(s_i, \Theta_{nf})$. It is calculated by adding together the weighted Probability Density Functions (PDFs) of every GMM component. The weight (w_{nf}, k), mean (μ_{nf}, k), and covariance (σ_{nf}, k, k) are assigned to each component k.

4) GenerateProbabilityMap Function

1. Based on the entered non-fatty liver samples, the function optimizes the GMM parameters (Θ_{nf}) utilizing the optimize GMMParameters function (using expectation maximization).
2. The probability values linked to each tumor are stored in a blank 3D array called the probability map.
3. Each tumor in the volume has its features extracted deploying the extractFeatures function.
4. Next, by employing the calculateGMMProbability function, the probability ($probability_{nf}$) of the tumor features corresponding to the GMM *nf* is determined.
5. The $probability_{nf}$ value is assigned to the matching tumor in the probability map.
6. Finally, the log probability estimate for each image is returned.

5) Multilevel Kernel Coefficient Index

The purpose of a multilevel kernel-correlation coefficient index for image filtering is to extract complex features that are highly informative for tasks such as disease identification or texture analysis. The kernel-correlation coefficient index serves as a foundational building block for this purpose, measuring the similarity between two sequences and providing a way to capture intricate patterns in the image data. This is particularly useful for identifying subtle variations in tumor textures or colors that may be indicative of a tumor condition. The kernel-correlation $Kc_{(p,q)}$ is given by:

$$Kc_{p,q}(l) = \sum_{m=-\infty}^{\infty} p\,(s) q^{*}(s-l) \quad (1)$$

where p and q are two sequences of size s samples, and l is the lag variable. The local adaptive kernel block image descriptor is :

$$L_{KD}(m,n) = \sum_{p=0}^{P-1} \sum_{q=0}^{Q-1} \boldsymbol{I}\,(i,j) \boldsymbol{K}^{*}_{\text{local}}\,(i-m, j-n) \quad (2)$$

where $K^{*}_{local}\,(i-m, j-n)$ is the conjugate complex of the local adaptive kernel at position $(i-m, j-n)$.

The goal is to extract complex features from these images that can be highly informative for tasks such as disease identification or texture analysis. In other words, the objective is to analyze tumor images to identify patterns or characteristics that may indicate a tumor. The kernel-correlation index can achieve these objectives. It is a mathematical function that measures the similarity between two sequences. In this context, it is used to capture intricate patterns in tumor image data. It is particularly useful for identifying subtle variations in tumor textures or colors, which can be indicative of a tumor condition. The local adaptive kernel block image descriptor is utilized to describe image content locally. It involves computing a sum of products between the input image *I* and a local adaptive kernel *K_* at different positions.

B. Multivariate Feature Extraction Measure

1) Multivariate Gaussian Mixture Model (GMM) Features

1. Initialize Variables.

   Input: Tumour features s_i, GMM parameters Θ_{nf}.

   Initialize: Probabilities $P_{nf}(s_i, \mu_{nf}, \sigma_{nf})$.
2. Calculate PDF.

   For each component k in GMM:

   $$pdf_k = N(x, \mu_k, \sigma_k) \quad (3)$$
3. Compute the weighted sum of PDFs.

   Compute probability P for block region features:

   $$P = \sigma_{kk} = w_k \cdot pdf_k \quad (4)$$
4. Optimize GMM parameters.

   Using expectation maximization:

   $$\Theta_{nf} *= argmax\Theta_{nf} \Pi T_i = GMM_{nf}(s_i; \Theta_{nf}) \quad (5)$$

2) Generative Probabilistic Map Features

1. Initialize variables.

   Input: Non-fatty liver samples.

   Initialize: GMM parameters Θ_{nf}, empty probability map.
2. Optimize GMM Parameters, using the optimizeGMMParameters function.
3. Calculate the probability for each tumor.

   For each tumor in the volume:

   $$probability_{nf} = calculateGMMProbability(tumourFeatures, \Theta_{nf})$$
4. Update the probability map.

   Assign $probability_{nf}$ to the corresponding tumor in the probability map.

C. Multivariate Feature Ranking Algorithm

Accurate identification and segmentation of liver tissue is made possible by multivariate joint probabilistic feature extraction approaches, which are essential in liver picture segmentation. These techniques enable precise segmentation by extracting pertinent characteristics using probabilistic models. A well-known method is the Hidden Markov Model (HMM), which shows a liver picture as a series of observable characteristics and hidden states. The underlying structure of the liver image is captured by hidden states, and the pixel values match the detected features. HMM efficiently divides liver tissue into discrete sections by computing the probability distribution of hidden states given the detected data. The Theta-regulated Gaussian Mixture Model (TGMM) is another notable technique. TGMM treats the liver image as a mixture of Gaussian distributions, each of which represents a distinct kind of liver tissue. To accurately segment tissues, it computes the liver image's probability distribution based on the detected features.

Furthermore, the Markov Random Field (MRF) model with theta control is employed for probabilistic feature extraction. This model views the liver image as a graph, in which the pixels are nodes and the edges stand in for spatial interactions.

Given the observed features, the MRF model determines a likelihood function and a prior distribution to compute the probability distribution of the image. The likelihood function evaluates the adherence to the prior distribution, whereas the prior distribution includes statistical features and spatial arrangement. By combining these components, the liver tissue is precisely segmented by the MRF model.

Using probabilistic models and distributions to improve the identification and segmentation of liver tissue, these probabilistic feature extraction techniques are extremely helpful in the segmentation of liver images.

1) Adaptive Kernel Gray Level Co-occurrence Matrix (KGLCM)

In the context of image analysis, the adaptive KGLCM method is deployed to capture complex texture patterns within an image. This method is particularly adaptive, adjusting its parameters based on the local characteristics of each pixel in the image. For each pixel, the method considers a local region around it, the size and orientation of which are determined by adaptive distance and direction parameters. These parameters are chosen based on the local spatial scale and texture orientation at each pixel, making the method highly sensitive to local variations. Within this local region, the method computes a matrix that captures the co-occurrence of intensity values between the central pixel and its neighbors. This matrix serves as a feature descriptor that encapsulates the local texture and intensity variations around each pixel. The adaptive nature of this method makes it highly versatile and effective for tasks that require capturing subtle and complex patterns, such as identifying tumors in medical images.

D. Multi-Variate Multi-Level Boosting Classifier

1) Proposed NL-SVM U-Net Model

The UNet architecture combined with a non-linear Support Vector Machine (SVM) is a powerful framework for liver tumor segmentation. This approach uses the strengths of deep learning for feature extraction and the robustness of SVM for classification, resulting in improved accuracy and efficiency.

a) Encoder Path

The encoder path follows a typical convolutional network structure. The convolutional layer applies convolution operations employing the ReLU activation function, and max pooling is utilized to down-sample the feature maps. Let X be the input image, and F_i be the feature maps at the i^{th} layer.

$$F_i = ReLU(Conv(F_i - 1)) \quad (6)$$

b) Decoder Path

The decoder path reconstructs the image using up-sampling. Up-sampling increases the resolution of the feature maps, concatenation is deployed to combine the up-sampled features with the corresponding features from the encoder path, and the convolutional layer applies convolution operations. Let U_i be the up-sampled feature maps at the i^{th} layer, and C_i be the concatenated feature maps:

$$U_i = UpSample(U_i + 1) \quad (7)$$

$$C_i = Concat(U_i, F_i) \quad (8)$$

c) Feature Extraction

After the UNet processes the input image, a high-dimensional feature vector H is obtained from the final layer of the encoder path. This feature vector serves as the input to the SVM classifier.

$$H = UNet(X) \quad (9)$$

d) Non-Linear SVM

The SVM classifier is trained to distinguish between tumor and non-tumor regions using the extracted features.

III. EXPERIMENTAL ANALYSIS

The 3D Image Reconstruction for Comparison of Algorithm Database (3DIRCADB) was used. The former is known for its diversity and complexity in liver and lesion images and consists of CT scans from different patients with a significant number of slices and expert segmentations provided by radiologists [20].

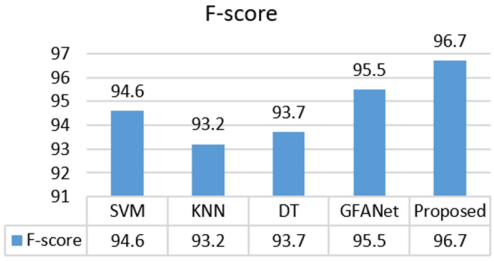

Fig. 2. Comparative analysis of the proposed LT segmentation-based classification approach and existing models using F-measure for noisy lesion detection on different heterogeneous images.

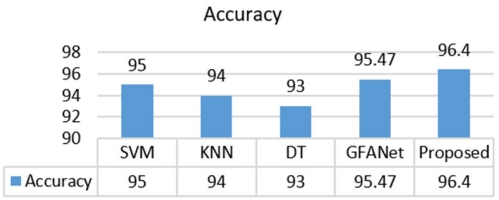

Fig. 3. Comparative analysis of the proposed LT segmentation-based classification approach and existing models using accuracy for noisy lesion detection on different heterogeneous data.

The F1 measure balances precision and recall in classification tasks. With an F-score of 96.7%, the proposed model performed best, successfully detecting and capturing liver tumors. With a 95.5% F1-score, the GFANet model exhibited good performance, indicating its efficacy in reducing false positives and negatives. The DT model obtained an impressive 93.7% F1 score, while the SVM model achieved 94.6%, demonstrating balanced precision and recall. The KNN model was reasonably accurate, although it had a slightly lower F1 score of 93.2%.

In classification tasks, accuracy measures the percentage of accurate predictions. With an accuracy of 96.4%, the proposed model was the most successful in detecting liver tumors. The GFANet model demonstrated reliability in liver tumor

identification, as it achieved 95.47% accuracy, followed by the SVM model at 95%. Despite being marginally less accurate than the others, the KNN model disclosed competence with an accuracy of 94%. With 93% accuracy, the DT model did well but trailed behind the others.

The capacity to distinguish positive cases from real positives is measured by evaluating different models according to their recall. With a recall of 96.8%, the proposed model was the best at detecting positive cases. The efficacy of GFANet and SVM was further evidenced by their strong recall values of 95.2% and 95%, respectively. Even with recall scores of 93.4%, KNN and DT demonstrated a high potential in detecting affirmative cases. These results show that while all models displayed reasonably good recall scores, indicating their efficacy in detecting liver tumors, the proposed model performed better in lesion detection than the other models.

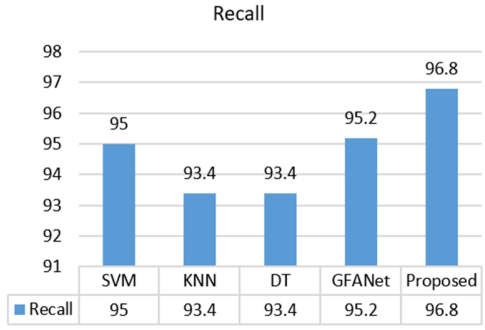

Fig. 4. Comparative analysis of the proposed LT segmentation-based classification approach and existing models using recall for noisy lesion detection on different heterogeneous data.

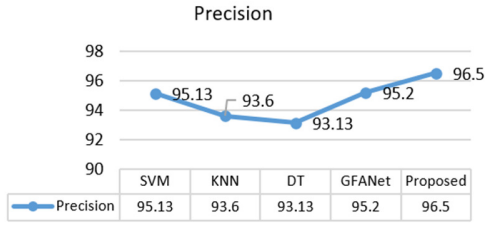

Fig. 5. Comparative analysis of the proposed LT segmentation-based classification approach and existing models using precision for noisy lesion detection on different heterogeneous data.

The proposed model had the best precision score of 96.5%. It was particularly good at detecting liver tumors and making accurate positive predictions. With a precision of 95.2%, GFANet also achieved good performance, demonstrating its efficacy in reducing false positives. With a precision of 95.13%, the SVM model demonstrated its ability to make accurate positive predictions. The KNN model achieved a precision of 93.6%, which was just below the top models. With a precision of 93.13%, the DT model was marginally less precise than the others, but it nevertheless demonstrated competency.

As evidenced in Figures 6 and 7, the proposed model performed well in detecting liver tumors, showing an error rate of 3.2% and an impressive accuracy of 96.8% with a fast runtime of 1934 ms. GFANet attained a 4% error rate, or 96% accuracy, with a respectable runtime of 2014 ms, designating it as a reliable choice. The SVM model manifested dependability in liver tumor diagnosis even with a 5% error rate and a slightly longer duration of 2132 ms. The KNN and DT models both showed error rates of 7%, but the former was marginally faster at 2043 ms.

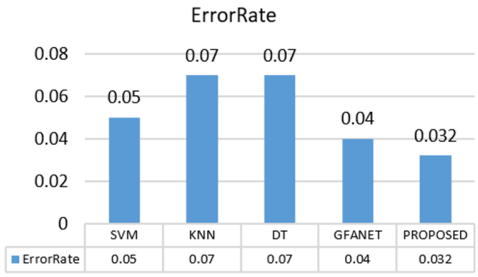

Fig. 6. Comparative analysis of the proposed LT segmentation-based classification approach and existing models using error rate for noisy lesion detection on different heterogeneous data.

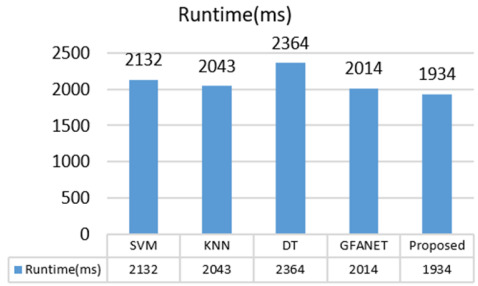

Fig. 7. Comparative analysis of the proposed LT segmentation-based classification approach and existing models using runtime (ms) for noisy lesion detection on different heterogeneous data.

IV. CONCLUSION

This study proposed a novel multiclass ensemble feature extraction and ranking deep learning architecture that enables real-time liver tumor diagnosis. The proposed model excelled in statistical metrics and runtime performance, addressing issues such as multi-modal tumor identification and segmentation noise. These findings demonstrate its potential for real-time detection of liver tumors, promising better diagnosis and treatment across diverse datasets. By improving tumor detection precision, the proposed framework promotes clinical practice and medical imaging. More studies in the detection and treatment of liver cancer could improve patient outcomes and healthcare delivery.

REFERENCES

[1] P. K. Mall *et al.*, "A comprehensive review of deep neural networks for medical image processing: Recent developments and future opportunities," *Healthcare Analytics*, vol. 4, Dec. 2023, Art. no. 100216, https://doi.org/10.1016/j.health.2023.100216.

[2] A. T. Tran, T. D. Luong, and V. N. Huynh, "A comprehensive survey and taxonomy on privacy-preserving deep learning," *Neurocomputing*, vol. 576, Apr. 2024, Art. no. 127345, https://doi.org/10.1016/j.neucom.2024.127345.

[3] B. Pandey, D. Kumar Pandey, B. Pratap Mishra, and W. Rhmann, "A comprehensive survey of deep learning in the field of medical imaging

and medical natural language processing: Challenges and research directions," *Journal of King Saud University - Computer and Information Sciences*, vol. 34, no. 8, Part A, pp. 5083–5099, Sep. 2022, https://doi.org/10.1016/j.jksuci.2021.01.007.

[4] R. Rong *et al.*, "A Deep Learning Approach for Histology-Based Nucleus Segmentation and Tumor Microenvironment Characterization," *Modern Pathology*, vol. 36, no. 8, Aug. 2023, Art. no. 100196, https://doi.org/10.1016/j.modpat.2023.100196.

[5] E. K. Wang, C. M. Chen, M. M. Hassan, and A. Almogren, "A deep learning based medical image segmentation technique in Internet-of-Medical-Things domain," *Future Generation Computer Systems*, vol. 108, pp. 135–144, Jul. 2020, https://doi.org/10.1016/j.future.2020.02.054.

[6] N. N. Prakash, V. Rajesh, D. L. Namakhwa, S. Dwarkanath Pande, and S. H. Ahammad, "A DenseNet CNN-based liver lesion prediction and classification for future medical diagnosis," *Scientific African*, vol. 20, Jul. 2023, Art. no. e01629, https://doi.org/10.1016/j.sciaf.2023.e01629.

[7] Y. Tian and S. Fu, "A descriptive framework for the field of deep learning applications in medical images," *Knowledge-Based Systems*, vol. 210, Dec. 2020, Art. no. 106445, https://doi.org/10.1016/j.knosys.2020.106445.

[8] H. Abdel-Nabi, M. Z. Ali, and A. Awajan, "A multi-scale 3-stacked-layer coned U-net framework for tumor segmentation in whole slide images," *Biomedical Signal Processing and Control*, vol. 86, Sep. 2023, Art. no. 105273, https://doi.org/10.1016/j.bspc.2023.105273.

[9] X. Kui *et al.*, "A review of dose prediction methods for tumor radiation therapy," *Meta-Radiology*, vol. 2, no. 1, Mar. 2024, Art. no. 100057, https://doi.org/10.1016/j.metrad.2024.100057.

[10] K. Zou, Z. Chen, X. Yuan, X. Shen, M. Wang, and H. Fu, "A review of uncertainty estimation and its application in medical imaging," *Meta-Radiology*, vol. 1, no. 1, Jun. 2023, Art. no. 100003, https://doi.org/10.1016/j.metrad.2023.100003.

[11] M. Abdar *et al.*, "A review of uncertainty quantification in deep learning: Techniques, applications and challenges," *Information Fusion*, vol. 76, pp. 243–297, Dec. 2021, https://doi.org/10.1016/j.inffus.2021.05.008.

[12] M. Aljabri and M. AlGhamdi, "A review on the use of deep learning for medical images segmentation," *Neurocomputing*, vol. 506, pp. 311–335, Sep. 2022, https://doi.org/10.1016/j.neucom.2022.07.070.

[13] S. Budd, E. C. Robinson, and B. Kainz, "A survey on active learning and human-in-the-loop deep learning for medical image analysis," *Medical Image Analysis*, vol. 71, Jul. 2021, Art. no. 102062, https://doi.org/10.1016/j.media.2021.102062.

[14] U. Ravindran and C. Gunavathi, "A survey on gene expression data analysis using deep learning methods for cancer diagnosis," *Progress in Biophysics and Molecular Biology*, vol. 177, pp. 1–13, Jan. 2023, https://doi.org/10.1016/j.pbiomolbio.2022.08.004.

[15] P. Deepa and C. Gunavathi, "A systematic review on machine learning and deep learning techniques in cancer survival prediction," *Progress in Biophysics and Molecular Biology*, vol. 174, pp. 62–71, Oct. 2022, https://doi.org/10.1016/j.pbiomolbio.2022.07.004.

[16] Y. Shui, Z. Wang, B. Liu, W. Wang, S. Fu, and Y. Li, "A three-path network with multi-scale selective feature fusion, edge-inspiring and edge-guiding for liver tumor segmentation," *Computers in Biology and Medicine*, vol. 168, Jan. 2024, Art. no. 107841, https://doi.org/10.1016/j.compbiomed.2023.107841.

[17] Z. Diao, H. Jiang, and T. Shi, "A unified uncertainty network for tumor segmentation using uncertainty cross entropy loss and prototype similarity," *Knowledge-Based Systems*, vol. 246, Jun. 2022, Art. no. 108739, https://doi.org/10.1016/j.knosys.2022.108739.

[18] S. M. Shaaban, M. Nawaz, Y. Said, and M. Barr, "An Efficient Breast Cancer Segmentation System based on Deep Learning Techniques," *Engineering, Technology & Applied Science Research*, vol. 13, no. 6, pp. 12415–12422, Dec. 2023, https://doi.org/10.48084/etasr.6518.

[19] N. Behar and M. Shrivastava, "A Novel Model for Breast Cancer Detection and Classification," *Engineering, Technology & Applied Science Research*, vol. 12, no. 6, pp. 9496–9502, Dec. 2022, https://doi.org/10.48084/etasr.5115.

[20] "Liver segmentation – 3D-IRCADb-01," *IRCAD*. https://www.ircad.fr/research/data-sets/liver-segmentation-3d-ircadb-01/.